Exploration of the Ionizable Metal Cluster–Electrode Surface Analogy: Infrared Spectroelectrochemistry of $[Pt_{24}(CO)_{30}]^n$, $[Pt_{26}(CO)_{32}]^n$, and $[Pt_{38}(CO)_{44}]^n$ (n = 0 to −10) and Comparisons with Potential-Dependent Spectra of CO Adlayers on Platinum Surfaces

Joseph D. Roth,[†] Gregory J. Lewis,[‡] Lance K. Safford,[†] Xudong Jiang,[†] Lawrence F. Dahl,*,[‡] and Michael J. Weaver*,[†]

Contribution from the Departments of Chemistry, Purdue University, West Lafayette, Indiana 47907, and University of Wisconsin—Madison, Madison, Wisconsin 53706. Received December 31, 1991

Abstract: Infrared spectroelectrochemistry has been utilized to explore the vibrational properties of the high-nuclearity platinum carbonyl clusters $[Pt_{24}(CO)_{30}]^n$, $[Pt_{26}(CO)_{32}]^n$, and $[Pt_{38}(CO)_{44}]^n$ as a function of the charge n in dichloromethane, acetonitrile, acetone, tetrahydrofuran, and methanol. The clusters exhibit unusually reversible voltammetric and spectroelectrochemical behavior, with a sequence of redox steps spanning n = 0 to (in one case) −10, having formal potentials, E_f, between ca. 0.5 and −2.5 V vs ferrocenium–ferrocene. Largely two-electron steps are observed for $[Pt_{26}(CO)_{32}]^n$, involving even-charge states (n = −2, −4, −6, −8, −10). Sequential one-electron steps are found for $[Pt_{24}(CO)_{30}]^n$ and $[Pt_{38}(CO)_{44}]^n$, although the regions of electrode potential over which odd-charge states (n = −1, −3, −5, −7) are stable (i.e., the spacings between E_f values) are markedly smaller than those for the even-charge states. The C–O stretching frequencies for the bridging (ν^b_{CO}) and especially the terminal (ν^t_{CO}) coordinated CO ligands decrease systematically as n becomes more negative; for example, ν^t_{CO} for $[Pt_{24}(CO)_{30}]^n$ diminishes by 15–20 cm⁻¹ per added electron. The observation of such remarkable charge-dependent spectral properties for these large and structurally well-defined platinum clusters invites comparisons with the potential (and consequent charge)-dependent properties of CO adlayers at corresponding platinum electrode–solution interfaces. The latter systems also display decreases in ν^t_{CO} and ν^b_{CO} as the electrode potential, E, and hence the surface charge is made more negative, as usually ascribed either to increased $d\pi$(Pt) → π^*(CO) backbonding or to a Stark effect. The ν^t_{CO}–E slopes for saturated CO adlayers at both single-crystal and polycrystalline Pt–nonaqueous interfaces are noticeably smaller than for the corresponding solvated Pt carbonyl clusters, the latter being adjudged from the ν^t_{CO}–E_f behavior. These differences are due chiefly to larger "effective surface" capacitances (i.e., charge–E_f dependencies) for the clusters than those measured for the electrode–solution interfaces. Such differing capacitances can largely be accounted for by a simple geometric electrostatic model. When the ν^t_{CO} values are plotted versus the electronic charge per surface Pt atom ("surface charge density"), however, an essentially uniform ν^t_{CO}–charge dependence is observed for the different Pt clusters, with similar behavior being obtained for the Pt electrodes. These comparisons provide an intriguing link between the electronic and bonding properties of such large ionizable metal clusters with those of chargeable metal surfaces.

The relationship between the properties of metal clusters and related metal surfaces has provided an enticing topic in chemistry for some time.[1] Besides solid-state materials, recent attention has been drawn to unraveling the size-dependent properties of gas-phase clusters.[2] In analogous fashion to gas-phase systems, many condensed-phase metal clusters exhibit relatively high electron affinities, i.e., easily become reduced to form anions. The stability of such charged species in solution is aided considerably by solvation factors, so that sequences of multiple charged anions might often be anticipated to be formed. Such species are particularly prevalent for clusters stabilized by π-acceptor ligands, most notably carbon monoxide.[1b,3]

The manner and ease by which metal–cluster reductions occur in solution, together with the changes thereby wrought upon the ligand properties, prompt additional interesting questions in the realm of cluster–surface analogies. Given that metal electrode–solution interfaces having coordinated adlayers (such as CO) can be charged simply by altering the electrode potential, how do the charge-induced alterations in surface–ligand and cluster–ligand bonding compare? More generally, what are the factors that control the potential-dependent behavior of metal–solution interfaces in relation to the charge-dependent properties of solution-phase metal clusters?

Despite their intriguing nature and fundamental significance to electrochemistry as well as to metal cluster chemistry, such issues have been virtually unexplored. It is desirable for this purpose to have at hand solution-soluble metal clusters, preferably of varying size and symmetry, which can be charged in a sequential fashion, i.e., exhibit a sequence of reversible (preferably one-

electron) redox steps. Carbonyl clusters are of particular interest in this regard since the C–O stretching frequency is well-known to be sensitive to the metal charge (or oxidation) state as well as the coordination geometry in cluster[3–6] as well as metal surface environments.[7]

An especially interesting example of such a system, which we have characterized recently by infrared spectroelectrochemistry,[6] is the high-nuclearity platinum carbonyl $[Pt_{24}(CO)_{30}]^n$.[3,5a] This cluster, isolated as the dianion, exhibits six reversible one-electron redox steps (involving n = 0 to −6) in dichloromethane as discerned

(1) (a) Muetterties, E. L.; Rhodin, T. N.; Band, E.; Brucker, C. F.; Pretzer, W. R. *Chem. Rev.* **1979**, *79*, 91. (b) Muetterties, E. L.; Wexler, R. M. *Surv. Prog. Chem.* **1983**, *10*, 61.
(2) (a) Kappes, M. M. *Chem. Rev.* **1988**, *88*, 369. (b) Cohen, M. L.; Knight, W. D. *Phys. Today* **1990**, December, 42.
(3) Kharas, K. C. C.; Dahl, L. F. *Adv. Chem. Phys.* **1988**, *70* (Part 2), p 1.
(4) For example: (a) Longini, G.; Chini, P. *J. Am. Chem. Soc.* **1976**, *98*, 7225. (b) Chini, P. *J. Organomet. Chem.* **1980**, *200*, 37. (c) Lauher, J. W. *J. Organomet. Chem.* **1981**, *213*, 25. (d) Clark, H. C.; Jain, V. K. *Coord. Chem. Rev.* **1984**, *55*, 151. (e) Teo, B. K. *J. Chem. Soc., Chem. Commun.* **1983**, 1362. (f) Mingos, D. M. P. *J. Chem. Soc., Chem. Commun.* **1985**, 1352. (g) Underwood, D. J.; Hoffmann, R.; Tatsumi, K.; Nakamura, A.; Yamamoto, Y. *J. Am. Chem. Soc.* **1985**, *107*, 5968. (h) Mingos, D. M. P. *Chem. Soc. Rev.* **1986**, *15*, 31. (i) Vargas, M. D.; Nicholls, J. N. *Adv. Inorg. Chem. Radiochem.* **1986**, *30*, 123. (j) Teo, B. K.; Sloane, N. J. A. *Inorg. Chem.* **1985**, *24*, 4545. (k) Mingos, D. M. P.; Zhenyang, L. *J. Chem. Soc., Dalton Trans.* **1988**, 1657. (l) Wales, D. J.; Stone, A. *Inorg. Chem.* **1989**, *28*, 3120.
(5) (a) Lewis, G. J. Ph.D. Thesis, University of Wisconsin, 1992. (b) Montag, R. A. Ph.D. Thesis, University of Wisconsin—Madison, 1982. (c) Washecheck, D. Ph.D. Thesis, University of Wisconsin—Madison, 1980.
(6) Lewis, G. J.; Roth, J. D.; Montag, R. A.; Safford, L. K.; Gao, X.; Chang, S.-C.; Dahl, L. F.; Weaver, M. J. *J. Am. Chem. Soc.* **1990**, *112*, 2831.
(7) For a recent overview, see: Chang, S.-C.; Weaver, M. J. *J. Phys. Chem.* **1991**, *95*, 5391.

[†] Purdue University.
[‡] University of Wisconsin.

by cyclic voltammetry.[6] Each redox form of $[Pt_{24}(CO)_{30}]^n$ yields remarkably characteristic infrared spectra, with C–O stretching frequencies for the terminal and bridging ligands, ν^t_{CO} and ν^b_{CO}, respectively, that downshift in near-linear fashion as n is made more negative.[6] Furthermore, the ν^t_{CO}–electrode potential (E) dependence for the cluster, associated with the sequence of formal potentials (E_f) for each redox step, displays an intriguing similarity to the corresponding ν^t_{CO}–E behavior for CO chemisorbed on a platinum electrode.[6] The infrared spectroelectrochemical approach offers the major virtue of providing both spectroscopic and electrochemical thermodynamic (E_f) information on the sequential charged cluster states, in closely analogous fashion to surface infrared spectra at metal electrodes.

These initial findings have encouraged us to explore in greater detail such charge-dependent infrared spectral behavior for $[Pt_{24}(CO)_{30}]^n$ and also for the related clusters $[Pt_{26}(CO)_{32}]^n$ and $[Pt_{38}(CO)_{44}]^n$ in several solvents in relation to the analogous behavior of electrosorbed CO on platinum surfaces. The resulting findings are reported herein. Additional, albeit less complete, spectral information for the larger clusters $[Pt_{44}(CO)_{47}]^{4-}$ and $[Pt_{50}(CO)_{48}]^{4-}$ is also utilized here. We have examined the infrared spectroelectrochemical properties in several solvents—dichloromethane, acetonitrile, acetone, tetrahydrofuran (THF), and methanol—chosen to provide a range of dielectric and solvating properties, in tetraalkylammonium and alkali metal supporting electrolytes. This cluster charge-dependent spectral behavior is compared here with analogous information also obtained by the Purdue group for adsorbed CO adlayers at low-index mono-crystalline[8,9] as well as polycrystalline[10] platinum surfaces. Taken together, the findings allow us to provide a uniquely detailed assessment of the charged metal cluster–surface analogy for these archetypical transition-metal carbonyl systems.

Experimental Section

The platinum carbonyl clusters examined here were synthesized as dianion salts as follows:[5a] [AsPh₄]₂[Pt₂₄(CO)₃₀]. A green-yellow THF solution containing [AsPh₄]₂[Pt₁₅(CO)₃₀][4a] was refluxed for 8 h under a light N₂ purge. The resulting brown solution was filtered from an insoluble black oil, concentrated under vacuum, and precipitated with hexane. The precipitate was then extracted with a THF/isopropyl ether solution and the extracts chromatographed on silica gel. The first fraction collected from the column was [AsPh₄]₂[Pt₂₄(CO)₃₀].

[AsPh₄]₂[Pt₂₆(CO)₃₂]. The black oil obtained from the reflux in the previous part was dissolved in acetonitrile and oxidized with an excess of ferrocenium hexafluoroantimonate. The resulting solution was filtered to another flask, concentrated under vacuum, and precipitated with iso-propyl ether. After this precipitate was washed with toluene it was extracted with THF/isopropyl ether solution and the extracts were chromatographed on silica gel. The first brown fraction collected from the column was [AsPh₄]₂[Pt₂₆(CO)₃₂].

[AsPh₄]₂[Pt₃₈(CO)₄₄]. [AsPh₄]₂[Pt₉(CO)₁₈][4a] was dissolved in CH₃CN and refluxed for 2 h under a light N₂ purge. After cooling, the brown solution was oxidized with a large excess of trifluoroacetic acid forming a grey precipitate. After the supernatant was filtered away, the precipitate was washed several times with cold acetonitrile, dissolved in THF–acetone (10:1 (v/v)), and chromatographed on silica gel. The first fraction contained [AsPh₄]₂[Pt₃₈(CO)₄₄] and usually some [Pt₂₆(CO)₃₂]²⁻ as an impurity. A few washes with cold acetonitrile removed the latter, leaving behind [AsPh₄]₂[Pt₃₈(CO)₄₄] as a grey precipitate.

The solvents used here were distilled under an atmosphere of nitrogen from the appropriate desiccant: dichloromethane from P₂O₅, acetonitrile from CaH₂, acetone from calcium sulfate, and THF from potassium metal with benzophenone. Methanol was reacted with Mg turnings to remove water *before* distillation. The supporting electrolytes were synthesized as follows. The tetramethylammonium, tetraethylammonium, and tetrabutylammonium perchlorates (TMAP, TEAP, TBAP) were prepared by the metathesis of the appropriate tetraalkylammonium bromide (Aldrich) and perchloric acid (Fisher) in water. The resulting TMAP, TEAP, and TBAP were recrystallized twice from water, and then ethanol, and methanol/water, respectively, and dried at 100 °C

under vacuum for 24 h. The corresponding tetraethylammonium hexa-fluorophosphate (TEAH) was prepared similarly by using ammonium hexafluorophosphate, and was recrystallized twice from absolute ethanol. The alkali perchlorates (LiClO₄, NaClO₄, from G.F. Smith) were re-crystallized twice from water and dried at 210 °C under vacuum.

The spectrometer was a Bruker/IBM IR 98-4A vacuum Fourier transform instrument, with a helical Globar light source and a liquid nitrogen-cooled narrow-band MCT detector. The spectral resolution was ±4 cm⁻¹. A spectroelectrochemical cell was employed that features a micrometer adjustment of the thin-layer thickness defined by the elec-trode–CaF₂ window separation and the provision of forced hydrodynamic flow.[12] The latter feature enables solutions to be replaced readily by flushing through the thin layer. The electrode was a 0.9 cm diameter gold disk. It was polished prior to use with 0.05-μm alumina, using water as a lubricant, and then sonicated for 15 min in the solvent to be used in the upcoming experiment. After the electrode was mounted in the infrared cell, cyclic voltammograms were recorded in the appropriate solvent containing only the supporting electrolyte to check the possible presence of water and other electroactive impurities. Provided that the voltammetric response was satisfactory, a reference infrared spectrum was then recorded and a platinum cluster-containing solution (typically ca. 0.7 mL containing ca. 5 mg of cluster) under nitrogen injected directly into the spectral thin layer. (This injection utilized a Pt tube entry through the CaF₂ window.[12]) Sequences of spectra were collected during the ensuing voltammetric potential excursions. Typically 5 interferometer scans (consuming ca. 2 s) were collected for each spectrum, the solvent and other spectral interferences being removed by subtracting the ref-erence spectrum obtained previously.

The electrode potentials were measured versus the ferrocenium–fer-rocene (Fc⁺/⁰) couple in the same solvent; this involved the use of an equimolar Fc⁺/Fc mixture in contact with a Pt wire, contained in a separate compartment. All measurements were made at room temper-ature, 23 ± 1 °C.

Results

The structures of the platinum carbonyl cluster anions utilized in this study are given in Figure 1. Figure 1A shows the structure of $[Pt_{24}(CO)_{30}]^{2-}$, which has a cubic closest packing of Pt atoms as is observed in the bulk metal.[5a,b] The cluster core, which conforms to pseudo C_{2v} symmetry, contains two mirror-related faces consisting of 10 coplanar Pt atoms, forming the largest "minisurfaces" among the clusters investigated here. The core also contains one 12-coordinate "bulk-like" Pt atom, as well as six 9-coordinate "terrace-like" surface atoms which bind a single terminal carbonyl. Inclusion of the 22 terminal and 8 doubly bridging carbonyl ligands lowers the pseudo C_{2v} Pt₂₄ core symmetry to C_2. The structure of $[Pt_{26}(CO)_{32}]^{2-}$, shown in Figure 1B, reveals a hexagonal closest packed (hcp), a:b:a, layered stacking of 7:12:7 Pt atoms in a cluster core of pseudo D_{3h} symmetry.[5a,c] Three Pt atoms, which form a triangle, are completely encapsulated within the cluster core, while there are two 9-coordinate and three 8-coordinate "terrace-like" surface atoms which bind a single ter-minal carbonyl. Inclusion of the 23 terminal and 9 doubly bridging carbonyl ligands lowers the pseudo D_{3h} Pt₂₆ core symmetry to mirror-plane C_s. The $[Pt_{38}(CO)_{44}]^{2-}$ structure, the core of which is shown in Figure 1C, possesses pseudo O_h symmetry and a cubic closest packed (ccp) arrangement of Pt atoms.[5c] Six Pt atoms which form an octahedron are totally encapsulated within the cluster core and are 12-coordinate, while eight Pt atoms have a 9-coordinate "surface" environment.

These clusters are particularly well-suited for exploring clus-ter/surface analogies. Thus the common packing motifs observed in bulk metals, ccp and hcp, are represented as well as "terrace-like" 9-coordinate metal atoms. The ability of such Pt carbonyls to emulate the structural features of bulk materials is in large part due to the d¹⁰ configuration of Pt. There is no great driving force to form additional Pt–CO rather than Pt–Pt bonds, accounting for the stability of these high-nuclearity clusters. The d¹⁰ configuration and low coordination requirement also allow the clusters to provide 9-coordinate surface sites where each Pt atom is bound to one terminal carbonyl as observed for Pt surfaces.

$[Pt_{24}(CO)_{30}]^n$. As described in preliminary fashion in ref 6, the basic experimental tactic employed here involves obtaining series of infrared spectra for the platinum carbonyl clusters as they

(8) Chang, S.-C.; Jiang, X.; Roth, J. D.; Weaver, M. J. *J. Phys. Chem.* **1991**, *95*, 5378.

(9) Jiang, X.; Weaver, M. J. *Surf. Sci.*, in press.

(10) Roth, J. D.; Weaver, M. J. *Langmuir* **1992**, *8*, 1451.

(11) Mann, C. K. In *Electroanalytical Chemistry—A Series of Advances*; Bard, A. J., Ed.; Marcel Dekker: New York, 1969; Vol. 3, p 57.

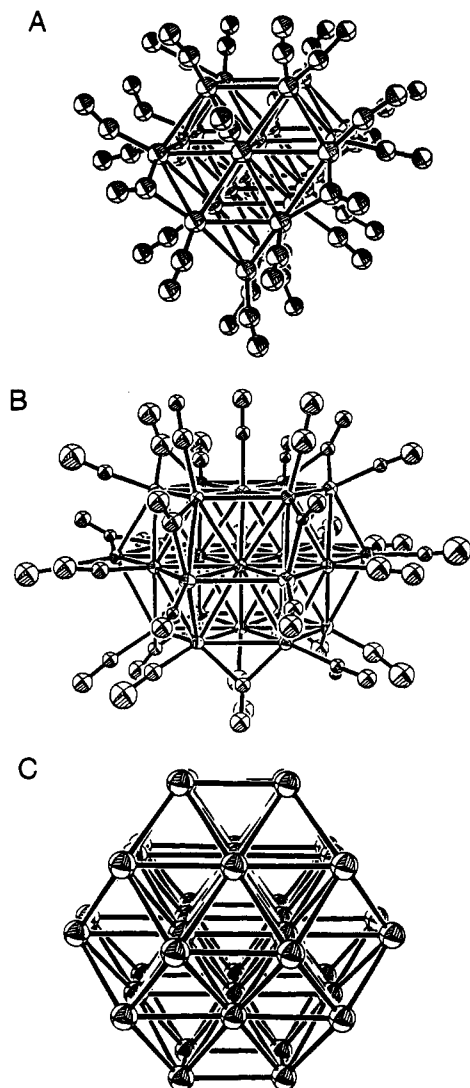(12) Roth, J. D.; Weaver, M. J. *J. Electroanal. Chem.* **1991**, *307*, 119.

A

B

C

Figure 1. Structures of platinum carbonyl clusters examined here:[5] (A) $[Pt_{24}(CO)_{30}]^{2-}$, featuring ccp metal core, with 22 terminal and 8 doubly bridging CO ligands. (B) $[Pt_{26}(CO)_{32}]^{2-}$, featuring hcp metal core, with 23 terminal and 9 doubly bridging CO ligands. (C) $[Pt_{38}(CO)_{44}]^{2-}$, only the ccp metal core is shown, since the CO coordination sites have not yet been ascertained due to a presumed crystal disorder.

undergo sequential electrochemical reduction and oxidation within the spectral thin layer. Most conveniently, this was accomplished by sweeping the potential at 5 mV s^{-1} through the accessible potential region. Initially negative-going sweeps from ca. 0 to −0.5 V vs Fc$^{+/0}$ were employed in most cases, sweep reversal being undertaken at various points following the reductions to check reversibility. Some potential sweeps were made initially in the positive direction in order to examine electrooxidation of the dianion unfettered by possible complications caused by preceding multiple electroreduction steps.

The spectral sequences obtained in this manner exhibit sharp potential-induced changes in ν_{CO} frequencies, reflecting the formation of successively more negatively charged (i.e., more highly reduced) clusters as the electrode potential is made progressively more negative. For $[Pt_{24}(CO)_{30}]^{n}$ in dichloromethane, as reported in ref 6, a sequence of one-electron steps from $n = 0$ to −6 was identified from cyclic voltammograms obtained separately in a conventional electrochemical cell with a Pt bead electrode (2 × 10^{-3} cm^2 area), using sweep rates from 0.05 to 1 V s^{-1}.[13] The

(13) Some electrochemical experiments at higher potential sweep rates using Pt and Au microelectrodes were also attempted, partly to expand the possible range of redox forms that could be examined. Serious difficulties, however, were encountered with the microelectrode response stability, probably arising from alterations in the surface morphology caused by cluster deposition and/or precipitation.
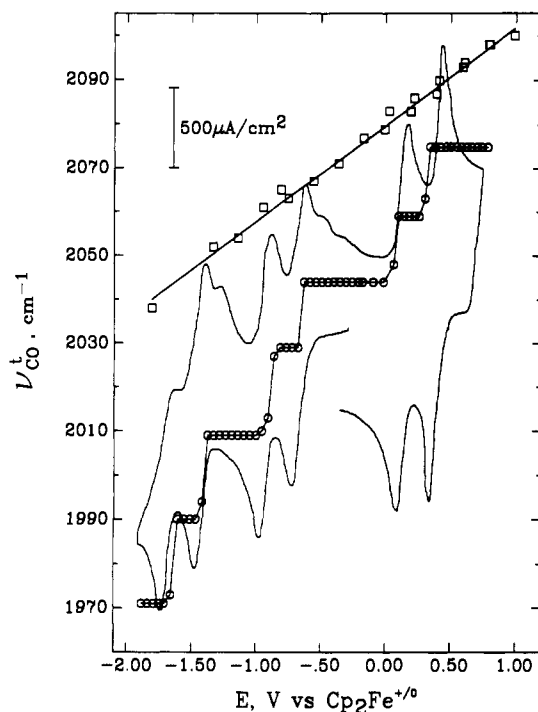

Figure 2. Comparison between infrared spectroelectrochemistry and cyclic voltammetry for $[Pt_{24}(CO)_{30}]^{n}$ in dichloromethane containing 0.3 M TBAP. The voltammogram (solid trace) was obtained at 0.1 V s^{-1} for 5 mM $[Pt_{24}(CO)_{30}]^{2-}$ using a Pt bead electrode. Circles are terminal C–O stretching frequency, ν_{CO}^{t}, for $[Pt_{24}(CO)_{30}]^{n}$ obtained from thin-layer spectroelectrochemistry plotted on a common potential scale, E. Squares are ν_{CO}^{t} versus E data (from ref 10) for the saturated CO adlayer on a polycrystalline Pt electrode in dichloromethane containing 0.3 M TBAP.

cathodic–anodic peak separations observed with iR compensation, 60–70 mV, together with the approximately equal amplitudes observed for the sequential voltammetric waves, provide strong evidence for the occurrence of uniformly one-electron steps. A typical cathodic–anodic cyclic voltammogram for 5 mM $[Pt_{24}-(CO)_{30}]^{2-}$ in dichloromethane containing 0.15 M TBAP is shown in Figure 2. A reasonable match was usually obtained between the potentials at which the sharp changes in the ν_{CO} frequency of the terminal ν_{CO} band, ν_{CO}^{t}, were observed and the occurrence of the voltammetric waves. This point is illustrated in Figure 2 by plotting the ν_{CO}^{t} values (open circles) obtained from the corresponding infrared spectra on a common electrode potential (E) scale. The ν_{CO}^{t}–E data shown were obtained during a 5 mV s^{-1} negative-going sweep. Closely similar ν_{CO}^{t}–E plots are obtained during the return (positive-going) sweep, although the potentials at which the ν_{CO}^{t}–E transitions occur tend to be significantly (20–100 mV) more positive, especially for the most negatively charged couples. Also included in Figure 2 (open squares) is a plot of ν_{CO}^{t} versus potential for a saturated CO adlayer on polycrystalline platinum in dichloromethane containing 0.3 M TBAP. (See ref 10 for details.) Comparable ν_{CO}^{t}–E dependencies are also obtained on ordered Pt(111) and Pt(110) electrode surfaces.[8,9] Note that the ν_{CO}^{t}–E behavior for the Pt metal–solution interface is roughly similar to, although clearly distinct from, that of the Pt cluster in solution.[6]

The spectroelectrochemical tactic therefore provides infrared data for a sequence of known cluster redox forms as well as yielding approximate formal potentials, E_f, at which the consecutive redox steps occur. Representative infrared spectra in the C–O stretching region obtained in this fashion for $[Pt_{24}(CO)_{30}]^{n}$ having various n values (−1 to −6) in acetonitrile and THF are shown in Figures 3 and 4. The former figure compares spectra obtained in THF and acetonitrile containing 0.15 M tetra-butylammonium perchlorate (TBAP) (Figure 3A and B, respectively). Only minor spectral differences are observed in these two solvents. Besides the characteristic intense terminal carbonyl
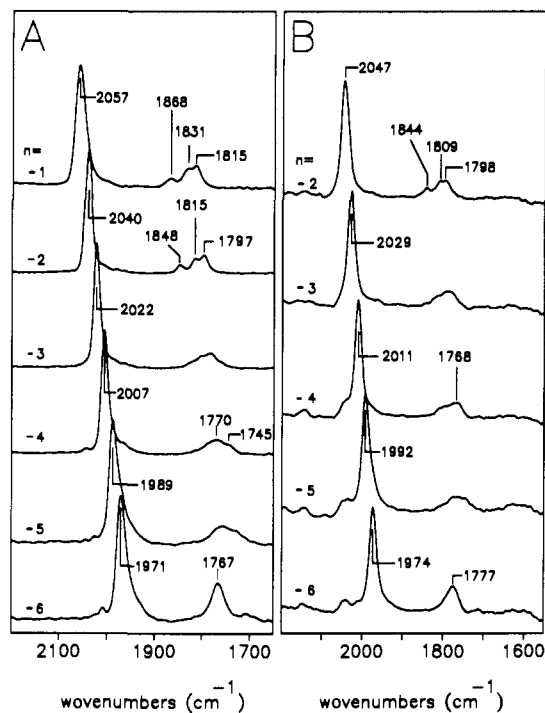
Figure 3. Selected infrared spectra for [Pt$_{24}$(CO)$_{30}$]^n as a function of the cluster charge, n, as indicated in (A) THF and (B) acetonitrile, containing 0.15 M TBAP. Each spectrum was generated from five interferometer scans acquired during a 5 mV s^{-1} potential sweep in a thin-layer spectroelectrochemical cell. A solvent blank, acquired immediately before injection of the cluster-containing solution into the thin layer, was used to subtract solvent, and supporting electrolyte, absorption interferences.
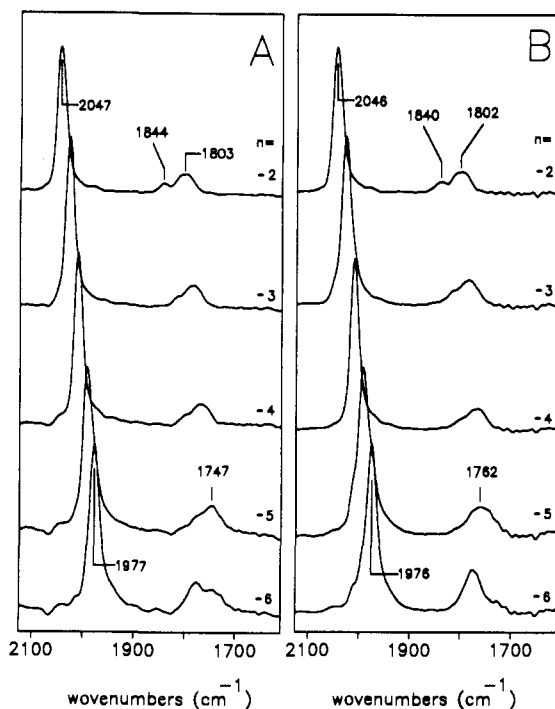

Figure 4. Spectra as in Figure 3, except for [Pt$_{24}$(CO)$_{30}$]^n in acetonitrile containing (A) 0.15 M NaClO$_4$ and (B) ~0.05 M TMAP.

band at ca. 1970–2060 cm^{-1}, a weaker bridging carbonyl feature at ca. 1770–1870 cm^{-1} is observed. While the frequencies of both these bands display a marked sensitivity to the cluster charge, the most clearcut trends are seen for the terminal feature in that ν_{CO}^t downshifts by 16–18 cm^{-1} for each added electron without exhibiting major changes in the intensity or bandshape. Figure 4 compares spectra obtained in acetonitrile containing sodium

Table I. Infrared ν_{CO} Frequencies and Relative Intensities for [Pt$_{24}$(CO)$_{30}$]^n in Selected Media as a Function of Cluster Charge n

medium[a]	cluster charge, n	ν_{CO}^t,[b] cm^{-1}	ν_{CO}^b,[c] cm^{-1}	A_{rel}^t[d]
dichloromethane +	0	2076	1885, 1850, 1830	22.1
0.3 M TBAP	−1	2061	1875, 1825, 1818	22.3
	−2	2045	1835, 1800	22.7
	−3	2028	1795	21.6
	−4	2010	1780	22.3
	−5	1991	1766	22.1
	−6	1973	1765	22.3
acetonitrile +	−2	2047	1845, 1810, 1800	22.5
0.15 M TBAP	−3	2029	1810, 1790	22.5
	−4	2011	1768	23.2
	−5	1992	1761	22.9
	−6	1972	1777	21.6
	−7	1950		
acetonitrile +	−1	2067	1868, 1826	22.8
0.15 M TEAP	−2	2047	1843, 1805	23.1
	−3	2029	1817, 1785	23.2
	−4	2011	1800, 1770	23.2
	−5	1992	1772, 1750	23.7
	−6	1974	1773	22.5
	−7	1951	1758	
acetonitrile +	−2	2046	1840, 1802	23.5
0.05 M TMAP	−3	2029	1813, 1785	23.7
	−4	2011	1767	24.3
	−5	1993	1762	23.8
	−6	1976	1775	23.4
acetonitrile +	−2	2047	1845, 1810, 1800	23.7
0.15 M NaClO$_4$	−3	2029	1815, 1785	24.3
	−4	2011	1800, 1770	24.0
	−5	1993	1775, 1745	23.3
	−6	1977	1777, 1745	21.4

[a] TBAP = tetrabutylammonium perchlorate; TEAP = tetraethylammonium perchlorate; TMAP = tetramethylammonium perchlorate. [b] Peak frequency of terminal C–O stretch. [c] Peak frequencies of bridging C–O stretch. [d] "Relative terminal band absorbance", obtained from $A_{rel}^t = [30A_t/(A_t + A_b)]$, where A_t and A_b are integrated absorbances of the corresponding terminal and bridging bands, respectively.

perchlorate and tetramethylammonium perchlorate (TMAP) electrolytes. While significant differences are seen in the charge-dependent frequencies and bandshapes for the bridging ν_{CO} band in these two electrolytes (vide infra), the terminal ν_{CO} band features are essentially identical.

We have reported earlier similar infrared spectra for [Pt$_{24}$(CO)$_{30}$]^n (n = 0 to −6) in dichloromethane.[6] The relative intensities of the terminal and bridging ν_{CO} features observed here are consistent with the 22 terminal and 8 bridging carbonyls present as deduced from the solid-state structure of [Pt$_{24}$(CO)$_{30}$]$^{2-}$ (Figure 1A).[7] The range of redox forms of [Pt$_{24}$(CO)$_{30}$]^n that could be examined spectroscopically is limited partly by the accessible potential ranges in each solvent, together with the cluster stability (and solubility). Thus, although clusters having charges as negative as −8 could be formed voltammetrically, there is insufficient stability (and probably solubility) beyond n = −6 to enable these reduction products to be examined reliably on the spectroelectrochemical time scale. The stable formation of the neutral cluster Pt$_{24}$(CO)$_{30}$ was most readily achieved in dichloromethane, although this species tended to deposit irreversibly on the electrode surface. The observed instability of the neutral species in more coordinating solvents such as acetonitrile is probably due to substitution of the CO ligands, which are bound more weakly toward higher oxidation states. Attempts to form positively charged clusters by sweeping to high positive potentials yielded only irreversible electrochemistry and resulted in cluster decomposition.

A summary of the ν_{CO} frequencies for [Pt$_{24}$(CO)$_{30}$]^n as a function of charge n in some selected media is given in Table I. A feature of these results is that the terminal ν_{CO} frequency for a given cluster charge is in most cases virtually independent of the solvent and the supporting electrolyte. (Similar frequencies

Table II. Formal Potentials, E_f, for $[Pt_{24}(CO)_{30}]^n$ Redox Couples in Various Solvents

medium[a]	redox couple	E_f,[b] V vs Fc$^{+/0}$
dichloromethane + 0.3 M TBAP	0/−1	0.4
	−1/−2	0.15
	−2/−3	−0.7
	−3/−4	−1.0
	−4/−5	−1.45
	−5/−6	−1.7
acetone + 0.15 M TBAP	−2/−3	−0.35
	−3/−4	−0.55
	−4/−5	−1.25
	−5/−6	−1.5
THF + 0.15 M TBAP	−1/−2	0.7
	−2/−3	−0.2
	−3/−4	−0.65
	−4/−5	−1.1
	−5/−6	−1.4
methanol + 0.15 M TBAP	−1/−2	0.15
	−2/−3	−1.4
	−3/−4	−1.75

[a] TBAP = tetrabutylammonium perchlorate. [b] Formal potential obtained (to nearest 0.05 V) from average of ν^t_{CO}–E transition potentials observed during 5 mV s^{-1} negative- and positive-going potential sweeps.

Table III. Formal Potentials, E_f, for $[Pt_{24}(CO)_{30}]^n$ Redox Couples in Acetonitrile Containing Various Supporting Electrolytes

electrolyte[a]	redox couple	E_f,[b] V vs Fc$^{+/0}$
0.15 M TBAP	−2/−3	−0.6
	−3/−4	−0.9
	−4/−5	−1.35
	−5/−6	−1.5
	−6/−7	−2.15
0.15 M TEAP	−1/−2	−0.1
	−2/−3	−0.65
	−3/−4	−0.9
	−4/−5	−1.4
	−5/−6	−1.55
	−6/−7	−2.3
0.05 M TMAP	−2/−3	−0.6
	−3/−4	−0.85
	−4/−5	−1.4
	−5/−6	−1.5
0.15 M NaClO$_4$	−2/−3	−0.6
	−3/−4	−0.85
	−4/−5	−1.35
	−5/−6	−1.5

[a] See Table I, footnote a, for symbol explanation. [b] See Table II, footnote b, for symbol explanation

were also obtained for the dianion in the absence of electrolyte.) As already noted, the frequencies (and bandshape) of the bridging ν_{CO} features are more sensitive to the solvent/electrolyte medium. Small yet discernable dependencies of ν^t_{CO} on the electrolyte cation are observed, however, for highly charged clusters; thus for $n = -6$, ν^t_{CO} increases by 5 cm^{-1} when Na$^+$ is substituted for TBA$^+$ (Table I). This effect is attributed to variations in the effective metal core charge resulting from site selective ion pairing. Also included in Table I are "relative terminal band absorbances", A^t_{rel}. This quantity is obtained from $A^t_{rel} = [30A_t/(A_t + A_b)]$, where A_t and A_b are the integrated absorbances of the terminal and bridging bands, respectively. (The factor of 30 is included to reflect the presence of 30 carbonyls, 22 terminal and 8 bridging, in the cluster.) The A^t_{rel} values are seen to be almost independent of the cluster charge and close to the value (22) expected if the absorptivities of the terminal and bridging bands are equal.

Tables II and III summarize formal potentials, E_f (vs Fc$^{+/0}$), for the various redox transitions observed spectroelectrochemically for $[Pt_{24}(CO)_{30}]^n$ in selected solvents containing TBAP and in acetonitrile containing various electrolytes, respectively. The values, which are quoted to the nearest 0.05 V, were obtained from the average between the ν^t_{CO}–E transitions observed during the negative-going and subsequent positive-going potential scans. The E_f values for a given redox couple, and the differences between values for successive redox transitions, are seen to be significantly solvent dependent in some instances (Table II). Thus the potential for dianion reduction in methanol is about 1 V more negative and the potential for oxidation of the dianion in THF is ca. 0.5 V more positive than in other solvents. Only small differences, however, are seen between the four electrolytes examined in acetonitrile (Table III). Nevertheless, use of lithium perchlorate in acetonitrile restricted the range of cluster stability to $-n \leq 4$; further reduction triggered irreversible cluster decomposition. An interesting general feature, which can also be discerned from the voltammogram in Figure 2, is that the potential ranges over which the odd charge states ($n = -1, -3, -5$) are stable (i.e., the differences between consecutive E_f values) are rather smaller than those for the even charge states ($n = -2, -4, -6$).

$[Pt_{26}(CO)_{32}]^n$ **and** $[Pt_{38}(CO)_{44}]^n$. Given the rich sequence of reversible redox transitions encountered for $[Pt_{24}(CO)_{30}]^n$, it is of interest to explore such behavior for the related clusters $[Pt_{26}(CO)_{32}]^n$ and $[Pt_{38}(CO)_{44}]^n$. Figure 5 shows a cathodic-anodic cyclic voltammogram at 0.2 V s^{-1} starting from −0.5 V for ca. 5 mM $[Pt_{26}(CO)_{32}]^{2-}$ in acetonitrile containing 0.15 M TEAP, using a Pt disk electrode. The voltammetry bears a similarity to that for $[Pt_{24}(CO)_{32}]^n$ in that a sequence of largely reversible redox transitions is seen toward more negative potentials.
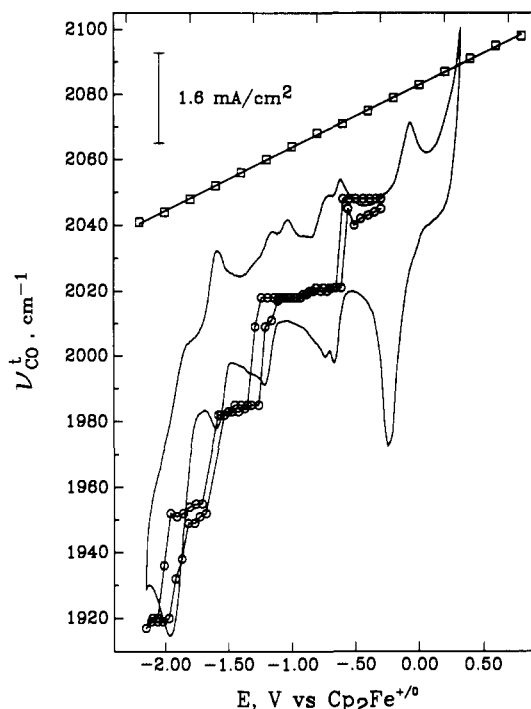

Figure 5. Spectra as in Figure 2, but for $[Pt_{26}(CO)_{32}]^n$ in acetonitrile containing 0.15 M TBAP. The cyclic voltammogram was obtained at 0.2 V s^{-1}. Spectroelectrochemical ν^t_{CO}–E data are shown for both forward (negative-going) and reverse (positive-going) potential sweeps. The squares are ν^t_{CO} versus E data (from ref 10) for the saturated CO adlayer on a polycrystalline Pt electrode in acetonitrile containing 0.15 M TBAP.

Similarly, the corresponding infrared spectroelectrochemical data for $[Pt_{26}(CO)_{32}]^n$ again exhibit a sequence of sharp ν^t_{CO}–E transitions at potentials that correlate well with the voltammetric waves. (These ν^t_{CO}–E data are plotted as open circles in Figure 5.) Illustrative spectra obtained for several such redox states of $[Pt_{26}(CO)_{32}]^n$ in THF and dichloromethane are shown in Figure 6A and B, respectively. The open squares in Figure 5 refer, as before, to corresponding ν^t_{CO}–E data obtained for a saturated CO adlayer on a polycrystalline platinum electrode in acetonitrile containing 0.15 M TBAP.

Closer inspection, however, of the voltammetric and spectroelectrochemical data for $[Pt_{26}(CO)_{32}]^n$ in Figure 5 reveals significant departures from the behavior of $[Pt_{24}(CO)_{30}]^n$ in Figure 2. In most cases the frequency downshifts associated with each
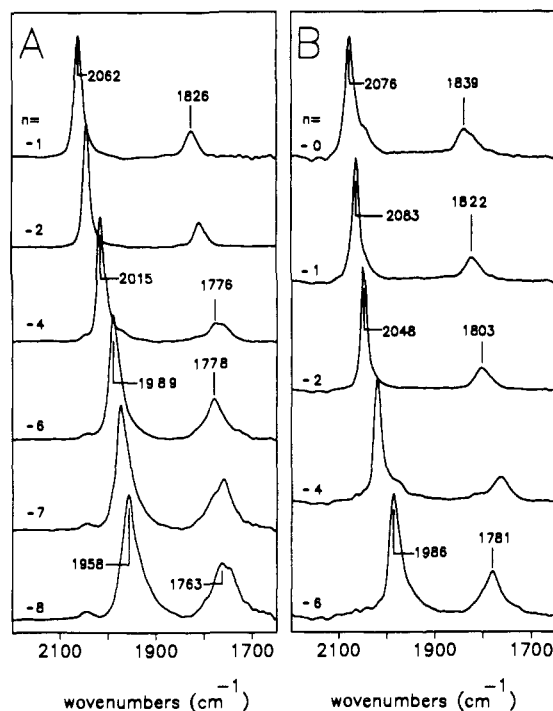
Figure 6. Spectra as in Figure 3, except for $[Pt_{26}(CO)_{32}]^n$ in (A) THF and (B) dichloromethane, containing 0.15 M TBAP.

$[Pt_{26}(CO)_{32}]^n$ reduction step are 30–35 cm^{-1}, i.e., about twice those observed for the $[Pt_{24}(CO)_{30}]^n$ system. This result suggests that these steps for $[Pt_{26}(CO)_{32}]^n$ involve two electrons, rather than one electron as for $[Pt_{24}(CO)_{30}]^n$. Deducing such information from the electrochemical data is less straightforward for $[Pt_{26}(CO)_{32}]^n$ since the voltammograms appear somewhat distorted, possibly due to the presence of decomposition products (compare the voltammograms in Figures 5 and 2). Nevertheless, better voltammetric data for the initial $[Pt_{26}(CO)_{32}]^{2-}$ reduction step could be obtained in some solvents by reversing the potential-sweep direction prior to the onset of the following cathodic wave. Under these conditions, a reversible-shaped voltammogram was obtained with a cathodic–anodic peak separation of 30–35 mV, virtually independent of the sweep rate, indicative of a two-electron step, i.e., involving the redox couple $[Pt_{26}(CO)_{32}]^{2-/4-}$.

By combining this information with the ν_{CO}^t–E data, it is apparent that $[Pt_{26}(CO)_{32}]^{2-}$ reduction occurs usually in a sequence of two-electron steps, i.e., involving formation of n = –4, –6, and –8. Evidently, then, the odd-numbered n states for $[Pt_{26}(CO)_{32}]^n$ tend to be less stable (with respect to disproportionation into the adjacent even-n states) by comparison with $[Pt_{24}(CO)_{30}]^n$. Nevertheless, on the basis of the observed ν_{CO}^t–E data for $[Pt_{26}(CO)_{32}]^n$, the odd-electron states n = –1 and –7 are detectable in some solvents (see Figure 6). In harmony with these observations, only the $[Pt_{26}(CO)_{32}]^n$ states n = –1, –2, –4, and –6 have been isolated synthetically.[5a]

A summary of the terminal and bridging ν_{CO} frequencies and relative terminal band intensities, A_{rel}^t, for $[Pt_{26}(CO)_{32}]^n$ as a function of n in selected solvents is provided in Table IV. (Note that now A_{rel}^t is defined as A_{rel}^t = $[32 A_t/(A_t + A_b)]$, reflecting the presence of 32 carbonyl ligands.) Similar to $[Pt_{24}(CO)_{30}]^n$, the ν_{CO}^t values for a given cluster charge are seen to be virtually independent of the solvent medium. As can be discerned from the illustrative spectra for $[Pt_{26}(CO)_{32}]^n$ in Figure 6, only a single bridging ν_{CO} feature is typically observed. Although its frequency tends to downshift with increasing cluster charge from n = 0 to –4, for more highly reduced clusters the bridging band tends to grow and also to upshift in frequency. This change is reflected in slightly smaller A_{rel}^t values for $-n$ > 5 (Table IV). Table V contains a summary of formal potentials for the various redox transitions for $[Pt_{26}(CO)_{32}]^n$ in various solvents, obtained as before from the spectroelectrochemical ν_{CO}^t–E data. Similarly to $[Pt_{24}(CO)_{30}]^n$, the E_f values for a given redox couple are seen to

Table IV. Infrared ν_{CO} Frequencies and Intensities for $[Pt_{26}(CO)_{32}]^n$ and $[Pt_{38}(CO)_{44}]^n$ in Selected Solvents as a Function of Cluster Charge n

cluster	medium[a]	cluster charge, n	ν_{CO}^t,[b] cm^{-1}	ν_{CO}^b,[c] cm^{-1}	A_{rel}^t[d]
$[Pt_{26}(CO)_{32}]^n$	dichloromethane + 0.15 M TBAP	0	2076	1839	25.3
		–1	2063	1822	26.2
		–2	2048	1803	24.8
		–4	2020	1764	25.0
		–6	1986	1781	21.7
	THF + 0.15 M TBAP	–1	2062	1826	25.4
		–2	2044	1809	25.3
		–4	2015	1776	24.5
		–6	1989	1778	22.2
		–7	1974	1761	21.6
		–8	1958	1763	21.0
	acetonitrile + 0.15 M TEAH	–2	2048	1803	26.1
		–4	2020	1768	26.1
		–6	1983	1769	25.3
		–8	1955	1769	21.7
		–10	1920	1741	22.7
$[Pt_{38}(CO)_{44}]^n$	dichloromethane + 0.15 M TBAP	–1	2068		
		–2	2058	1804	34.0
		–3	2044		
		–4	2033		
		–5	2022		
		–6	2010		
		–7	1997		

[a] TBAP = tetrabutylammonium perchlorate. [b] Peak frequency of terminal C–O stretch. [c] Peak frequency of bridging C–O stretch. [d] "Relative terminal band absorbance", obtained from A_{rel}^t = $[mA_t/(A_t + A_b)]$, where A_t and A_b are the integrated absorbances of the corresponding terminal and bridging bands, respectively, and m equals the number of carbonyl cluster ligands.

Table V. Formal Potentials, E_f, for $[Pt_{26}(CO)_{32}]^n$ and $[Pt_{38}(CO)_{44}]^n$ Redox Couples in Various Solvents

cluster	medium[a]	redox couple	E_f,[b] V vs Fc$^{+/0}$
$[Pt_{26}(CO)_{32}]^n$	dichloromethane + 0.15 M TBAP	0/–1	0.4
		–1/–2	0.1
		–2/–4	–0.85
		–4/–6	–1.4
	THF + 0.15 M TBAP	–1/–2	0.85
		–2/–4	–0.15
		–4/–6	–0.85
		–6/–7	–1.35
		–7/–8	–1.6
	acetonitrile + 0.15 M TEAH	–2/–4	–0.6
		–4/–6	–1.2
		–6/–8	–1.7
		–8/–10	–2.3
	methanol + 0.15 M TBAP	–1/–2	0.2
		–2/–4	–0.65
$[Pt_{38}(CO)_{44}]^n$	dichloromethane + 0.15 M TBAP	0/–1	0.5
		–1/–2	0.25
		–2/–3	–0.8
		–3/–4	–0.9
		–4/–5	–1.2
		–5/–6	–1.35
		–6/–7	–1.8

[a] See Table IV, footnote a, for symbol explanation. [b] Determined as noted in Table II, footnote b.

depend significantly, and in some cases substantially, on the solvent medium.

A more restricted examination was made of the infrared spectroelectrochemistry of $[Pt_{38}(CO)_{44}]^n$. (A synthesis was designed only recently which yielded material sufficiently pure for spectroelectrochemical measurements.[5a]) Nevertheless, a well-defined spectral data set was obtained in dichloromethane and is summarized in Figure 7. Once again, sharp ν_{CO}^t–E transitions
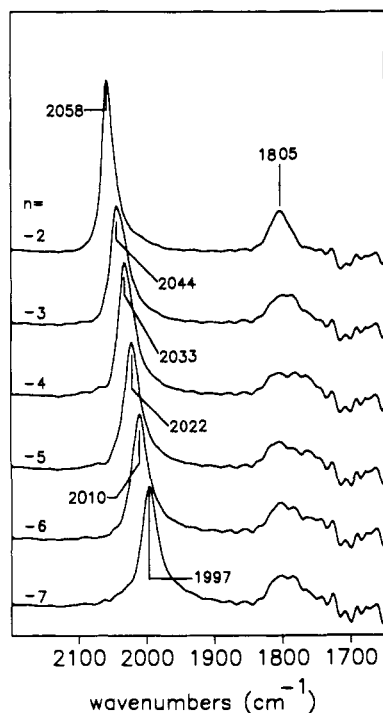
The Ionizable Metal Cluster–Electrode Surface Analogy

J. Am. Chem. Soc., Vol. 114, No. 15, 1992 6165

Figure 7. Spectra as in Figure 3, except for $[Pt_{38}(CO)_{44}]^n$ in dichloromethane containing 0.15 M TBAP.

Figure 8. Comparison between ν_{CO}^t–E data for saturated CO adlayers on polycrystalline Pt (open circles) and Pt(110) (open triangles) in dichloromethane containing 0.3 and 0.15 M TBAP, respectively, with analogous ν_{CO}^t–E data for $[Pt_{24}(CO)_{30}]^n$ (filled upright triangles), $[Pt_{26}(CO)_{32}]^n$ (filled squares), and $[Pt_{38}(CO)_{44}]^n$ (filled inverted triangles) in dichloromethane containing 0.15 M TBAP. The cluster ν_{CO} values are the average frequencies between adjacent redox states (n values), plotted at $E = E_f$ for each redox step.

were obtained. While insufficient sample was available to permit complete voltammetric characterization, one-electron transfers are indicated on the basis of the relatively small (11–14 cm^{-1}) incremental ν_{CO}^t decreases associated with each reduction step. The resulting n values are noted alongside each spectrum in Figure 7. The ν_{CO}^t values are also listed in Table IV. Included in Table V are the corresponding E_f values for $[Pt_{38}(CO)_{44}]^n$ in dichloromethane extracted, as before, from the ν_{CO}^t–E data. Similar to $[Pt_{24}(CO)_{30}]^n$, the odd-n redox forms are seen to be stable only over narrow (0.1–0.25 V) potential ranges in comparison with the even-n forms. This observation, indeed, supports the above assignment of cluster charges for $[Pt_{38}(CO)_{44}]^n$.

Discussion

As already noted, of central interest here is the analysis of the charge-dependent spectroelectrochemical properties of the platinum carbonyl clusters in relation to corresponding potential-dependent information for CO adlayers on platinum surfaces. In order to pursue such ionizable metal cluster–charged surface analogies, it is clearly desirable to know the relationship between the electrode potential and charge for the metal surfaces under consideration. The excess electronic charge density, σ_m, present on a metal electrode can be varied continuously by altering the electrode potential away from the so-called potential of zero charge, E_{pzc}, where by definition $\sigma_m = 0$.

It is often difficult to measure E_{pzc} for reactive metal surfaces such as platinum, especially in aqueous media where surface redox processes abound. Nevertheless, approximate E_{pzc} estimates have been obtained for CO-covered platinum electrodes in the nonaqueous media examined here by evaluating ν_{CO}^t–E data in a given solvent containing tetraalkylammonium cations of varying sizes.[8–10] At negative electrode charges (as are encountered here), cations will populate the so-called outer Helmholtz plane (oHp), so that the distance over which the potential drop occurs (within the inner part of the double layer) should be determined in part by the cation radius.[14] Small yet significant decreases in the ν_{CO}^t–E slopes are indeed observed as the cation radius increases, which can be understood in terms of the diminishing fraction of the interfacial potential drop located across the CO adlayer under these con-
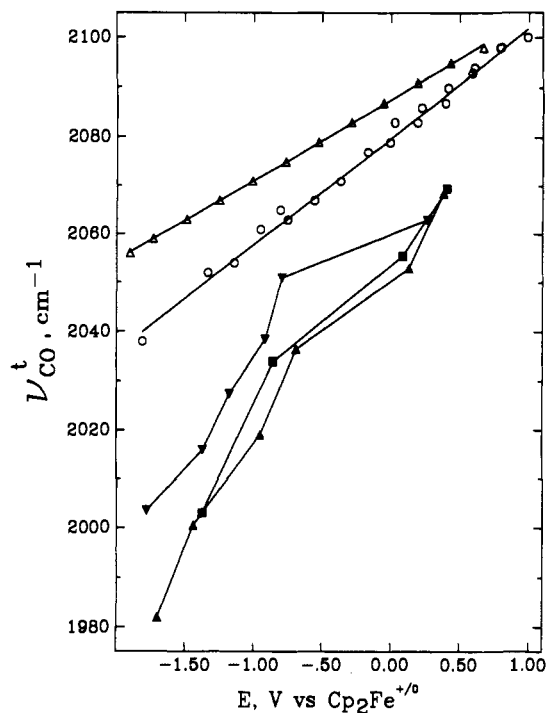
ditions.[8–10] (This result is discussed further below.) The intersection potential of these ν_{CO}^t–E plots should approximate E_{pzc} since the free-charge contribution to the double-layer potential will thereby be zero. This procedure yields E_{pzc} estimates of 0.5 V vs Fc$^{+/0}$ for polycrystalline Pt and Pt(110)[9,10] and 0.7 V for Pt(111)[8] in acetonitrile; similar values are also obtained in other solvents.

Consequently, then, the CO-covered platinum surfaces become increasingly negatively charged as the electrode potential is lowered below ca. 0.5 V vs Fc$^{+/0}$ in a given solvent. It is interesting to note that the addition of the first electron to the neutral clusters $Pt_{24}(CO)_{30}$, $Pt_{26}(CO)_{32}$, and $Pt_{38}(CO)_{44}$ occurs at a similar electrode potential (vs Fc$^{+/0}$) as discerned by the E_f values for the 0/–1 redox couples in dichloromethane (Tables II and V). This finding supports the notion that the ν_{CO} frequency downshifts for adsorbed CO induced by lowering the platinum electrode potential have a similar (or the same) origin as the frequency shifts for carbonyl ligands produced by electrochemically reducing the platinum clusters. These potential (or charge)-induced ν_{CO} frequency shifts have been rationalized in terms of increased dπ(Pt) → π*(CO) backbonding for both metal cluster[4a,15] and electrode surface[16] cases. The observed adsorbate frequency shifts for the latter have also often been described in terms of a field-induced first-order Stark effect.[17] The two models appear to be in part complementary,[7] although a consensus in the surface chemistry community as to their relative validity has not yet been reached.[7,16a,17]

Figure 8 is a comparison between the ν_{CO}^t–E behavior observed for saturated CO adlayers on polycrystalline Pt and ordered Pt(110) electrodes in dichloromethane (open circles and triangles, respectively) with the analogous ν_{CO}^t–E dependencies for [Pt$_{24}$-

(14) For a readable introduction to these basic concepts in surface electrochemistry, see: Bockris, J. O'M.; Reddy, A. K. N. *Modern Electrochemistry*; Plenum: New York, 1970; Vol. 2, Chapter 7.
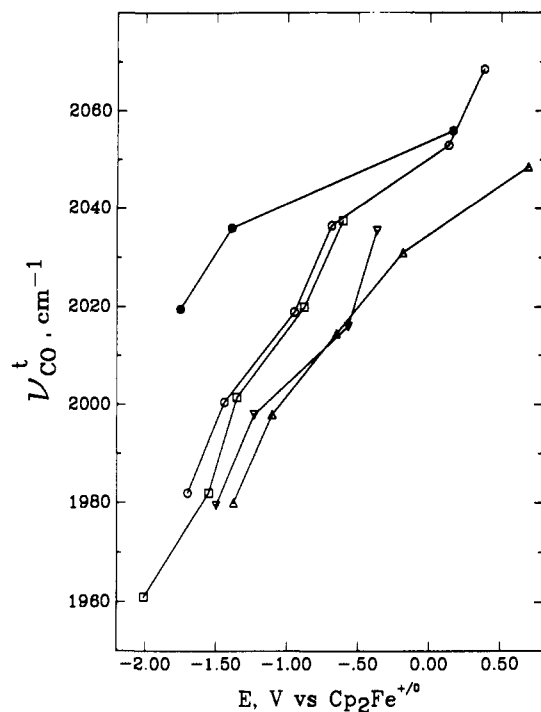
(15) Cirjak, L. M.; Ginsburg, R. E.; Dahl, L. F. *Inorg. Chem.* **1982**, *21*, 940.

(16) (a) Anderson, A. B. *J. Electroanal. Chem.* **1990**, *280*, 37. (b) Mehandru, S. P.; Anderson, A. B. *J. Phys. Chem.* **1989**, *93*, 2044.

(17) For example: Lambert, D. K. *J. Chem. Phys.* **1988**, *89*, 3847 and previous references cited therein.

Figure 9. Comparison between ν^t_{CO}–E plots for $[Pt_{24}(CO)_{30}]^n$ in various solvent media. As in Figure 8, the ν^t_{CO} values are the average frequencies between adjacent cluster redox states (n values), plotted at $E = E_f$ for each redox step: open circles, dichloromethane/0.3 M TBAP; open squares, acetonitrile/0.15 M TBAP; open upright triangles, THF/0.15 M TBAP; open inverted triangles, acetone/0.15 M TBAP; filled circles, methanol/0.15 M TBAP.

Figure 10. Plot of ν^t_{CO} for the various Pt carbonyl clusters versus the excess electronic charge per surface Pt atom: open upright triangles, $[Pt_{24}(CO)_{30}]^n$ in dichloromethane/0.3 M TBAP; open inverted triangles, $[Pt_{24}(CO)_{30}]^n$ in acetonitrile/0.15 M TBAP; open circles, $[Pt_{26}(CO)_{32}]^n$ in dichloromethane/0.15 M TBAP; open squares, $[Pt_{26}(CO)_{32}]^n$ in acetonitrile/0.15 M TBAP; filled circles, $[Pt_{38}(CO)_{44}]^n$ in dichloromethane/0.15 M TBAP; filled square, $[Pt_{44}(CO)_{47}]^{4-}$ in THF. The solid line segment (and extrapolated dashed line) is for a saturated CO adlayer on Pt(111), obtained from ν^t_{CO}–E and electrode capacitance data as outlined in the text.

$(CO)_{30}]^n$ (filled upright triangles), $[Pt_{26}(CO)_{32}]^n$ (filled squares), and $[Pt_{38}(CO)_{44}]^n$ (filled inverted triangles), also in dichloromethane. The surface infrared data are taken from refs 9 and 10 and the cluster data from Tables I, II, IV, and V. For convenience, the latter (inevitably quantized) ν^t_{CO}–E data are plotted as the *average* ν^t_{CO} values between adjacent cluster redox states at potentials equal to E_f for each redox couple, with straight lines drawn between each such redox transition. This format provides ν^t_{CO}–E data for the clusters in an analogous fashion to the metal surfaces.

Inspection of Figure 8 shows that the downshifts in ν^t_{CO} for the clusters induced by lowering the electrode potential are markedly greater than those observed at polycrystalline Pt, or especially at Pt(110). [Corresponding ν^t_{CO}–E data for Pt(111) exhibit behavior intermediate between these two surfaces.[8]] Interestingly, however, the largest cluster, $[Pt_{38}(CO)_{44}]^n$, exhibits an ν^t_{CO}–E dependence which is somewhat intermediate between that for the smaller clusters and the "infinitely large clusters", i.e., the metal surfaces. This result therefore suggests that the cluster size plays an important role in controlling the potential-dependent CO binding properties.

Before pursuing this issue further, it is appropriate to note in this context the observed specific solvent effects upon E_f, pointed out above. Figure 9 contains plots of ν^t_{CO} versus E, in the same format as Figure 8, for $[Pt_{24}(CO)_{30}]^n$ in the various solvents examined here containing TBAP. (These data were taken largely from Tables I and II.) This figure shows graphically the substantial deviations of ν^t_{CO}–E behavior obtained in THF (upright triangles) and especially in methanol (filled circles). In the case of THF, the solvent appears to interact specifically with the $[Pt_{24}(CO)_{30}]^n$ cluster as adjudged by the significantly (4–5 cm⁻¹) lower ν^t_{CO} values for $n = -2$ and -1 than those observed in other solvents. While the charge-dependent ν^t_{CO} values for $[Pt_{24}(CO)_{30}]^n$ in methanol are not significantly different from those obtained in other media, a substantially smaller ν^t_{CO}–E slope is indicated from Figure 9. The reasons for these specific solvent effects are somewhat unclear. It is feasible that cluster aggregation is responsible, aided by ion pairing with electrolyte cations; this is
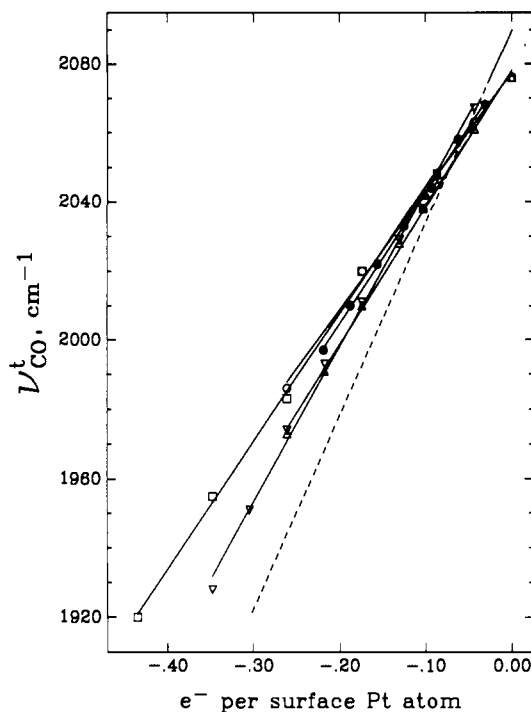
anticipated in solvents in which the cluster solubility is limited, such as methanol. The formation of such aggregates would diminish the solvation energy that stabilizes the more highly charged clusters, accounting for the anomalously negative dianion reduction potential in methanol.

Nevertheless, the near-uniform observation that essentially solvent-independent ν^t_{CO} values are obtained for a given cluster charge state indicates that these differences in ν^t_{CO}–E behavior between different clusters and in different solvents are due largely to variations in the charge–E_f dependencies, i.e., in the effective "surface capacitance" of the cluster. Given the likelihood that the excess electronic charge is delocalized around the surface Pt atoms present in the cluster, this suggests that it is fruitful to examine the relationship between ν^t_{CO} and the cluster "surface-charge density" σ_{mc}. Most simply, σ_{mc} can be defined in terms of the number of excess electrons per surface Pt atom in the cluster. From the structures in Figure 1A–C, the total number of surface Pt atoms in $Pt_{24}(CO)_{30}$, $Pt_{26}(CO)_{32}$, and $Pt_{38}(CO)_{44}$ is 23, 23, and 32, respectively. Figure 10 contains ν^t_{CO}–σ_{mc} plots for $[Pt_{24}(CO)_{30}]^n$ (open triangles), $[Pt_{26}(CO)_{32}]^n$ (open circles, squares), and $[Pt_{38}(CO)_{44}]^n$ (filled circles). Data are included for the first two clusters in both dichloromethane and acetonitrile to expand the total range of charge states. Also shown are ν^t_{CO} values for $[Pt_{44}(CO)_{47}]^{4-}$ and $[Pt_{50}(CO)_{48}]^{4-}$; these larger clusters have recently been isolated and characterized in Madison.[5a]

Inspection of Figure 10 shows that the ν^t_{CO}–σ_{mc} behavior is intriguingly uniform, closely similar or even near-coincident linear plots being obtained for all five clusters. This finding is remarkable in that it indicates that the Pt–CO bonding properties are determined largely by the local metal charge density, irrespective of cluster size. Admittedly, such uniform behavior may reflect in part the close structural relationship between the various Pt clusters examined here. It is therefore of considerable interest to compare such ν^t_{CO}–σ_{mc} behavior with analogous ν^t_{CO}–σ_m data for CO adlayers on Pt surfaces.

In order to pursue such comparisons, it is necessary to have information on the differential surface capacitance, C_s ($= d\sigma_m/dE$), since this quantity (as a function of E) along with E_{pzc} allows the observed ν_{CO}^t–E data to be transposed into ν_{CO}^t–σ_m plots. Measurements of C_s on transition-metal electrodes are usually not straightforward, partly since interferences from faradaic surface processes are common. Nevertheless, approximate C_s–E data were successfully obtained for CO-covered Pt(111) and Pt(110) in acetonitrile containing 0.1 M TBAP. Over the potential range ca. 0 to -1.0 V vs Fc$^{+/0}$, where most satisfactory results were obtained, C_s was found to be largely independent of potential and equal to 6 ($\pm$1) μF cm^{-2} at both surfaces.[18] This quantity can be transformed readily into the required capacitance per surface Pt atom by noting that an ordered Pt(111) surface contains 1.5 $\times$ 10^{15} atoms cm^{-2}.

A resulting ν_{CO}^t–σ_m plot for a saturated CO adlayer on Pt(111), extracted from the corresponding ν_{CO}^t–E data in acetonitrile given in ref 8 along with C_s = 6 μF cm^{-2}, is included in Figure 10 as the solid-line segment (top right-hand corner); this is linearly extrapolated to more negative potentials by means of the dashed line. Considering the uncertainties involved in the capacitance measurements, the corresponding surface ν_{CO}^t–σ_m and cluster ν_{CO}^t–σ_{mc} plots are deemed to be in reasonable concordance. Comparable ν_{CO}^t–σ_m behavior is also obtained for the Pt(110)/CO system.

It is notable that the span of σ_m values accessed within the electrode potential range considered here, ca. 0.5 to -2.5 V vs Fc$^{+/0}$, is considerably smaller for the Pt surfaces than for the clusters. For the former, σ_m varies from ca. 0 to 0.075 e$^-$/surface Pt, whereas for the latter, σ_{mc} ranges from 0 to about 0.45 e$^-$/surface Pt. These differences can be viewed as inferring that the "surface capacitance" of the Pt clusters, C_s, tends to be larger (per unit area) than that for the planar interfaces themselves. This disparity can also be discerned from the charge–E_f data in Tables III and V. For both [Pt$_{24}$(CO)$_{30}$]^n and [Pt$_{26}$(CO)$_{32}$]^n, the charge–E_f dependencies are roughly 3 e$^-$ per V. Assuming that the Pt atoms pack as at a Pt(111) surface, the charge–E_f dependence corresponds to a C_s value of ca. 30 μF cm^{-2}. This value, however, is probably an overestimate; while most of the planar Pt facets on these clusters involve hexagonal close packing [as on Pt(111)], the rows of the Pt atoms on the facet edges contribute more to the surface area than would be the case at a planar interface. Taking an average cluster radius of about 5 Å (yielding a surface area of 3.1 $\times$ 10^{-14} cm^2) leads to an effective C_s value about 2-fold smaller, ca. 15 μF cm^{-2}. A similar cluster surface area can also be obtained by summing the individual contributions from each planar facet in the cluster crystallographic structure.

While C_s values of this magnitude are not uncommon for electrochemical surfaces, smaller values (in the range ca. 5–10 μF cm^{-2}) are usually obtained at metal–nonaqueous interfaces, especially at negative electrode charges, consistent with the present value of ca. 6 μF cm^{-2} for CO-covered Pt(111) and Pt(110). It is interesting to speculate briefly on the possible reasons for these larger C_s values observed for the present clusters. At least part of the difference can be accounted for in terms of simple electrostatics. The clusters may be viewed roughly as spherical-shaped conductors with effective (metallic) radii, r_c, 4.5–6 Å. Provided that the potential drop surrounding such spheres is confined to comparable distances, d_c,[20] one can deduce on electrostatic grounds that C_s values that are 2 to 3-fold larger than for a parallel-plate

(i.e., conventional surface) capacitor, with inner-layer thickness d_i, will be obtained.[21] Still larger cluster C_s values relative to the plane-surface case are anticipated if $d_c < d_i$. (This analysis will be pursued in greater detail in a forthcoming paper.)

In this connection, it is interesting to note that quite different effects of varying the electrolyte cation upon the ν_{CO}^t–E behavior are obtained in the cluster and surface cases. For the latter, as mentioned above, significant decreases in the ν_{CO}^t–E slopes are observed as the cation size increases;[8-10] for example, $d\nu_{CO}^t/dE$ on polycrystalline Pt in acetonitrile decreases from ca. 26 to 19 cm^{-1} V^{-1} when substituting TBAP for TMAP electrolyte.[10] These variations are consistent with the decreases in d_i expected from the usual double-layer model, given that the cation radius should determine in part the oHp location (vide supra).

Significantly, however, the ν_{CO}^t–E (or charge–E_f) dependencies for [Pt$_{24}$(CO)$_{30}$]^n in acetonitrile containing TBAP, TEAP, and TMAP do not differ appreciably. (This can be discerned by carefully inspecting Tables I and II.) The electrostatic environment around the charged Pt clusters evidently differs somewhat from that at the corresponding surfaces, suggesting that the cation countercharge is located at significantly different sites in the two cases. One possibility is that the charged clusters feature electrolyte cations meshed somewhat between the carbonyl ligands. This is sterically feasible, especially at Pt edge sites, given the high curvature of the cluster surfaces. Evidence for some specific interaction between the cluster carbonyl ligands and the cation countercharges is provided by the small yet appreciable upshifts in ν_{CO}^t observed for [Pt$_{24}$(CO)$_{30}$]^n, when $-n > 4$, as the tetra-alkylammonium cation size decreases (Table I). The charged planar Pt surfaces, on the other hand, offer little opportunity for the cationic countercharge to penetrate the close-packed CO adlayer. Consequently, there is some reason to anticipate that $d_c < d_i$, thereby rationalizing in part the higher C_s values observed for the Pt clusters.

While we have focussed so far on the nonspecific geometric factors that may influence the properties of the Pt clusters in comparison with planar surfaces, some features of the present results point to the discrete microscopic nature of the former systems. Most evident for [Pt$_{24}$(CO)$_{30}$]^n and [Pt$_{38}$(CO)$_{44}$]^n are the smaller potential regions over which the odd-electron states (i.e., $n = -1, -3, -5, -7$) are stable in comparison with the even-electron forms of the clusters. Thus, the spacings between adjacent E_f values alternate between small (0.1–0.3 V for $n = -1, -3, -5, -7$) and larger (ca. 0.5–1 V for $n = -2, -4, -6$) values (Tables II, III, and V). Moreover, for [Pt$_{26}$(CO)$_{32}$]^n the odd-electron states ($n = -3, -5, -7$) tend to be unstable with respect to disproportionation, so that concerted *two*-electron steps are commonly observed, involving the adjacent even-electron states $-2/-4$, $-4/-6$, and $-6/-8$ (Table V). This alternating degree of electronic stability can most simply be attributed to orbital filling, whereby the added electrons enter successive LUMO's in a pairwise fashion. Interestingly, the effect is analogous to the so-called "even–odd" ionization effects observed for gas-phase clusters, whereby higher ionization potentials and lower electron affinities are observed for neutral clusters containing even numbers of metal atoms.[2a,23]

Another interesting, if somewhat complex, feature of the present Pt clusters concerns the n-dependent behavior of the bridging ν_{CO} bands. For [Pt$_{24}$(CO)$_{30}$]^n, three distinct bridging carbonyl bands can often be resolved for $-n \leq 2$ (Figure 3), presumably associated with the three types of bridging CO seen in the crystallographic

(18) The measurements involved the use of ac impedance with a lock-in amplifier, largely as described in ref 19. The ordered single crystals were prepared by a flame-annealing procedure as noted in ref 8. After introducing the electrode into solution, the saturated CO adlayer was formed by solution sparging. (The formation of close-packed CO adlayers using this procedure is confirmed by means of infrared spectroscopy.[8,9]) The measured C_d values were found to be stable and independent of the ac frequency (within 10–15%) over the range 10–200 Hz.

(19) Hupp, J. T.; Larkin, D.; Weaver, M. J. *Surf. Sci.* **1983**, *125*, 429.

(20) This rough estimate arises from the "thickness" of the CO ligands around the cluster metal core together with the screening of the metal charge provided by the surrounding electrolyte cations, yielding an ionic atmosphere which sets the outer boundary to the metal cluster–solution potential drop.

(21) For a spherical capacitor of radius r_c surrounded by a concentric outer shell [of radius ($r_c + d_c$)], between which the potential drop is confined in a medium of dielectric constant ϵ_s, the capacitance per unit area is given by the following (in c.g.s. units):[22] $C_s = \epsilon_s(r_c + d_c)/4\pi d_c r_c$; the corresponding parallel-plate capacitor formula is $C_s = \epsilon_s/4\pi d_i$, where d_i is now the electrochemical inner-layer thickness. If $d_c = d_i$ and for a given ϵ_s, the factor by which the cluster capacitance is enhanced above the plane surface value is therefore simply ($r_c + d$)/r_c.

(22) For example: Rojansky, V. *Electromagnetic Fields and Waves*; Prentice-Hall: Englewood Cliffs, NJ, 1971; p 277.

(23) Leopold, D. G.; Ho, J.; Lineberger, W. C. *J. Chem. Phys.* **1987**, *86*, 1715.
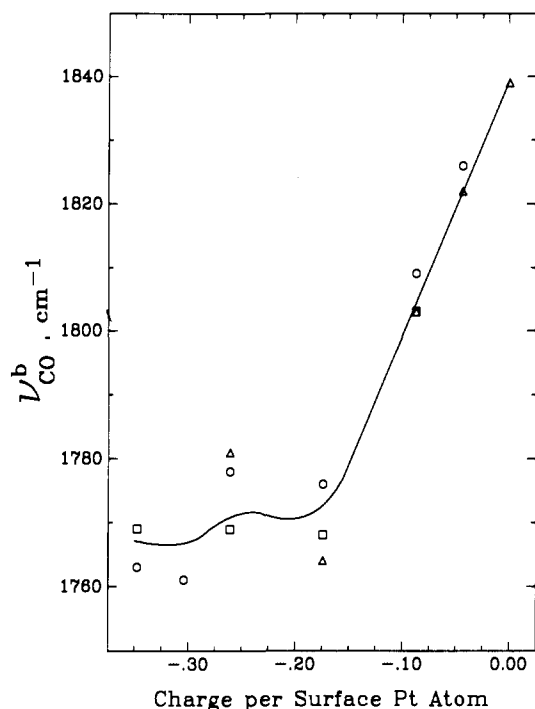
Figure 11. Plot of ν_{CO}^{b} for $[Pt_{26}(CO)_{32}]^{n}$ versus the excess electronic charge per surface Pt atom. Triangles, circles, and squares refer to data obtained in dichloromethane/0.15 M TBAP, THF/0.15 M TBAP, and acetonitrile/0.15 M TEAP, respectively.

structure (Figure 1A). For higher cluster charges, however, these bands tend to coalesce into a single feature. Also, while the ν_{CO}^{b} values tend to downshift progressively as $-n$ increases, an upshift is observed for $-n > 6$. The latter is also seen clearly for $[Pt_{26}-(CO)_{32}]^{n}$, as shown in Figure 11 in the form of a $\nu_{CO}^{b}-E$ plot. These effects are probably due to the local electrostatic fields created by cluster charging, along with interactions with the cation countercharges. Structural rearrangements may well occur, involving changes in the bridging CO bonding interactions.

These observations have no obvious parallel in the corresponding potential-dependent behavior of CO adlayers on Pt electrodes. Nevertheless, a closer analogy in this regard is observed for $[Pt_{26}(CO)_{32}]^{n}$ in that the A_{rel}^{t} values are seen to decrease significantly as $-n$ increases (Table IV); i.e., the bridging ν_{CO} feature becomes more intense relative to the terminal ν_{CO} band at higher cluster charges. In addition, the terminal band broadens under these conditions (Figure 6). These observations strongly suggest that the added electronic charge induces a significant shift in ligand geometry from terminal to bridging sites. A qualitatively similar charge-induced effect is commonly observed for saturated (and also lower-coverage) CO adlayers on low-index platinum and rhodium electrodes.[7,8,24] This progressive stabilization of bridging versus terminal CO binding can be rationalized in terms of the increased degree of $d\pi(M)-2\pi^{*}(CO)$ backbonding expected at higher negative charges.[7,16]

Nevertheless, while this charge-induced site occupancy shift is observable for $[Pt_{26}(CO)_{32}]^{n}$, it is only evident at large σ_{mc} values and is essentially absent for $[Pt_{24}(CO)_{30}]^{n}$ and $[Pt_{38}(CO)_{44}]^{n}$, at least for n values where the clusters are stable toward decomposition. This relatively high stability of the cluster structures toward ligand isomerization is probably due to the rigidity imparted by the carbonyl close packing. It is noteworthy that the CO fractional coverages, θ_{CO} (i.e., the number of CO ligands per surface Pt atom), are well above unity (ca. 1.3) for the present clusters, as compared with the sub-unity values found for saturated CO adlayers on low-index Pt surfaces in both electrochemical and gas-phase environments.[7]

It is also appropriate to comment briefly on the behavior of the present Pt carbonyl clusters in relation to CO adlayers on Pt

surfaces in ultrahigh vacuum (uhv). In general, the latter systems can be perceived as being uncharged (i.e., $\sigma_{m} = 0$) in the absence of ionizable coadsorbates.[7] Generally, saturated CO adlayers on low-index Pt surfaces yield slightly higher ν_{CO} frequencies than those obtained for the uncharged Pt clusters. For example, for Pt(111)/CO ($\theta_{CO} \approx 0.7$), $\nu_{CO}^{t} = 2102$ cm^{-1} and $\nu_{CO}^{b} = 1887$ cm^{-1}.[25] Both these ν_{CO} frequencies (especially the latter) are known to be sensitive to the local steric environment, associated with dynamic dipole coupling and other local interaction effects.[26] Significantly, very similar ν_{CO} frequencies (and relative band intensities) are observed for the corresponding Pt surfaces in nonaqueous electrochemical environments at potentials corresponding to $\sigma_{m} = 0$ (i.e., at E_{pzc}).[8,9] The slightly different behavior of the Pt clusters in this regard is therefore most likely due to the dissimilar local environments surrounding the carbonyl ligands compared with CO bound to the planar Pt surfaces.

Concluding Remarks

The rich spectroelectrochemical behavior exhibited by the present high-nuclearity platinum carbonyls provides a clear demonstration of the opportunities that such reversible redox systems offer for exploring charged metal cluster–surface analogies. As such, the present findings have significant implications in both cluster chemistry and surface electrochemistry. The ability of the present high-nuclearity clusters to accept electrons in reversible stepwise fashion to reach negative charge densities as high as ca. 0.4 e^{-} per surface Pt attests to their remarkable electronic nature. While their charge-dependent spectroelectrochemical properties still deviate significantly from those of planar Pt surfaces, the differences can be understood partly in terms of geometric effects, whereby the larger effective capacitance of the metal clusters can be understood in terms of their (roughly) spherical nature. Such factors presumably more than offset the effect of the HOMO-LUMO orbital spacings, which will tend to diminish the capacity to add additional electrons for a given incremental change in electrode potential due to the progressively increasing orbital energies.

These cluster properties are also of significance to surface electrochemistry in that they provide novel information on the manner in which the charge-dependent properties of such larger molecular systems converge to those for planar metal electrodes. Given that clusters containing more than 50–100 metal atoms are commonly thought to be required in order for their electronic properties to approach those of metal surfaces,[3] the observed differences in the $\nu_{CO}^{t}-E$ behavior between the clusters and surfaces (Figure 8) are not surprising. The significant feature in this regard is the markedly greater degree to which ν_{CO}^{t} for the cluster carbonyls is downshifted by negative potential alterations in comparison with the behavior of CO adlayers on Pt electrodes. The clusters therefore provide a means of inducing greater potential-dependent alterations in ligand bonding than are exhibited by planar metal surfaces. Besides its intrinsic significance, this finding suggests that interesting differences in potential-dependent binding may occur for adsorbates bound at rough (or undulating) metal surfaces, if these indeed contain small crystallites that can mimic the behavior of discrete metal clusters. It would certainly be of interest in this regard to examine the spectral properties of electrode surfaces containing deposited metal clusters.

Nevertheless, the commonality of the $\nu_{CO}^{t}-\sigma_{mc}$ plots observed not only for all the clusters but also when $\nu_{CO}^{t}-\sigma_{m}$ data for Pt(111) are included (Figure 10) attests to the close similarity in the Pt–CO bonding for all these systems when viewed in terms of the metal atomic *charge*. Such a finding, although quite notable, can be rationalized in terms of the likely "local" nature of the metal–CO bonding. Consequently, then, there appears to be a clear distinction between *potential-* and *charge*-dependent bonding properties of metal clusters and metal electrodes. The former, but not the latter, characteristics are sensitive to the surface

---

(24) Chang, S.-C.; Weaver, M. J. *Surf. Sci.* **1990**, *238*, 142.

(25) Persson, B. N. J.; Tüshaus, M.; Bradshaw, A. M. *J. Chem. Phys.* **1990**, *92*, 5034.

(26) For example: Tüshaus, M.; Schweizer, E.; Hollins, P.; Bradshaw, A. M. *J. Electron. Spectrosc. Relat. Phenom.* **1987**, *44*, 305.

geometry as discerned from the effective capacitance, yielding interesting behavioral trends in cluster size and differences between clusters and surfaces.

Overall, then, there is reason to conclude that the exploration of the "ionizable metal cluster–electrode surface" analogy is capable of yielding substantial fresh insight into the behavior of both types of systems. We describe elsewhere an examination of the Pt carbonyl clusters in comparison with Pt/CO surfaces with regard to the issue of CO dipole coupling, as examined by means of $^{12}CO/^{13}CO$ substitution.[27] While the high-nuclearity platinum

(27) Roth, J. D.; Lewis, G. J.; Jiang, X.; Dahl, L. F.; Weaver, M. J. *J. Phys. Chem.*, in press.

carbonyls offer redox properties that are so far unparalled for metal clusters, there are a wealth of other systems that can also be examined in this fashion to good effect. One such study, for nickel carbonyls, will be reported elsewhere.

The Stability of Bridgehead and Rigid Tertiary Carbenium Ions in the Gas Phase and Their Rate of Formation in Solvolysis Reactions

Paul Müller,*,† Didier Milin,† Weiging Q. Feng,‡ Raymond Houriet,‡ and Ernest W. Della§

Contribution from the Département de Chimie Organique, Université de Genève, CH-1215 Genève, Switzerland, Institut de Chimie Physique, Ecole Polytechnique Fédérale (EPFL), CH-1015 Lausanne, Switzerland, and the School of Physical Sciences, The Flinders University of South Australia, Bedford Park, South Australia 5042, Australia. Received January 16, 1992

Abstract: The gas-phase stability of bridgehead and rigid tertiary carbenium ions has been measured by equilibria for bromide transfer and equilibria for protonation of olefins by ICR techniques. Combination of the experimental data with the MM2-calculated enthalpies of formation of the neutrals gives the enthalpy change associated with the ionization process. The rate constants for solvolysis of the corresponding tertiary halides and sulfonate esters correlate linearly with these enthalpy changes. However, simple acyclic and monocyclic tertiary derivatives exhibit higher solvolytic reactivities than expected on the grounds of the thermodynamics of the reaction.
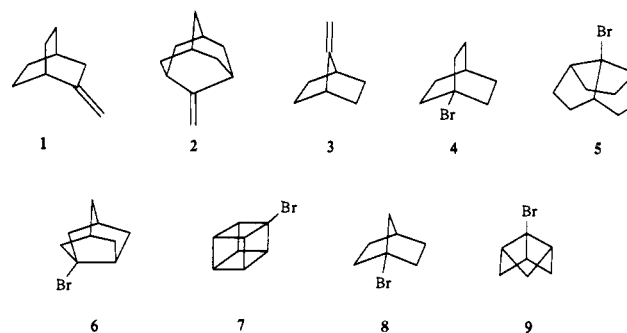
Introduction

The interpretation of the rate constants of solvolysis of tertiary halides and sulfonate esters is a topic of long-standing interest in physical organic chemistry. Indeed, much of our present knowledge of the properties of carbenium ions is derived from solvolysis reactions.[1] For these reactions it is usually assumed that the transition state occurs late on the reaction coordinate so that, according to the Hammond postulate,[2] the intermediate carbenium ion may be assumed to be similar with respect to structure and energy. Based on this hypothesis, force field calculations have been performed to evaluate the strain difference between substrate and carbenium ion,[3] and the strain differences of some 50 bridgehead or other rigid tertiary substrates have been correlated with their rates of solvolysis. A satisfactory correlation over the entire rate range of ca. 25 log units was obtained.[4,5]

Since the force field calculations are empirical, and since the carbenium ion force field has been adjusted such as to achieve the best possible fit with the rate constants for solvolysis, the validity of the underlying hypothesis of geometric and energetic equivalency between transition state and intermediate in solvolysis reactions is not established by these strain–reactivity correlations. We have now determined the intrinsic stabilities of some strained tertiary carbenium ions in the gas phase in order to establish the thermodynamics of the ionization process.

Experimental Section

(a) **Gas-Phase Experiments.** Gas-phase stabilities were determined from equilibrium experiments from proton or bromide transfer reactions

† Université de Genève.
‡ Institut de Chimie Physique.
§ The Flinders University of South Australia.

Scheme I

conducted in an ion cyclotron (ICR) spectrometer.[6] Proton transfer equilibrium reactions between olefins 2-methylenebicyclo[2.2.2]octane (1), 2-methyleneadamantane (2), and 7-methylenenorbornane (3) yielded the gas-phase basicity (GB) according to the reaction:

$$MH^+ + B \rightleftarrows M + BH^+ \qquad (1)$$
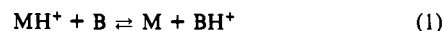
(1) Fort, R. C. In *Carbonium Ions*; Olah, G. A., Schleyer, P. v. R., Eds.; Wiley: New York, 1972; Vol. IV, Chapter 32.
(2) Hammond, G. S.; Hogle, D. H. *J. Am. Chem. Soc.* **1955**, *77*, 334.
(3) (a) Bingham, R. C.; Schleyer, P. v. R. *J. Am. Chem. Soc.* **1971**, *93*, 3189. (b) Parker, W.; Tranter, R. L.; Watt, C. I. F.; Chang, L. W. K.; Schleyer, P. v. R. *Ibid.* **1974**, *96*, 7121.
(4) Müller, P.; Mareda, J. *J. Comput. Chem.* **1989**, *10*, 863. Müller, P.; Mareda, J. In *Cage Hydrocarbons*; Olah, G. A., Ed.; Wiley: New York, 1990.
(5) Müller, P.; Milin, D. *Helv. Chim. Acta* **1991**, *74*, 1808.
(6) Bollinger, J. C.; Houriet, R.; Kern, C. W.; Perret, D.; Weber, J.; Yvernault, T. *J. Am. Chem. Soc.* **1985**, *107*, 5352.